Short-range order and pair potentials in Au-Ag

B. Schönfeld, J. Traube, and G. Kostorz

Institut für Angewandte Physik, Eidgenössische Technische Hochschule Zürich, CH-8093 Zürich, Switzerland

Au-Ag single crystals with 25, 48, and 75 at. % Ag in a state of thermodynamic equilibrium frozen in by quenching were investigated by diffuse x-ray scattering. The elastic-scattering contributions due to short-range order and static atomic displacements were separated using the method of Borie and Sparks and of Georgopoulos and Cohen. Weak short-range-order maxima were always found at 100 positions. The effective pair potentials determined by an inverse Monte Carlo method as well as by the high-temperature approximation of Clapp and Moss are dominated by the nearest-neighbor interaction of 10–16 meV. Based on these pair potentials, the superstructures $L1_0$ and $L1_2$ are found as stable low-temperature phases. For the stoichiometric compositions Monte Carlo simulations give order-disorder transitions at 100–200 K.

INTRODUCTION

The microstructure of gold-silver alloys has attracted much attention over the years. Based on measurements of the electrical resistivity,[1-3] a central issue was whether the short-range order is best described by the statistical model using short-range-order parameters[4] or by the model of "disperse order."[5] Whereas short-range order is distributed evenly over the whole sample within the former model, the latter model assumes a fine dispersion of highly ordered domains within a disordered matrix. Since electrons are then expected to experience an additional scattering up to a certain size of the ordered regions, an increase in electrical resistivity after certain heat treatments seemed to fit this model (the microstructure is then often termed the K state[6]).

The electrical resistivity does not allow the atomic structure to be unequivocally deduced. Much more detailed information may be obtained by evaluating data (based on short-range-order coefficients) from diffuse scattering experiments. For the interpretation of such data in the gold-silver system, however, the model of disperse order was also used;[7] as no distinct difference in diffuse scattering was found in samples with different thermal histories (samples were either irradiated with 2-MeV electrons at 328 K up to 33 h or aged at 473–573 K) the statistical model seemed inappropriate. These measurements were, however, restricted to a $(h_1 h_2 0)$ plane of reciprocal space. Furthermore, several experimental difficulties were met, like an unsatisfactory quality of the surface or the somewhat shifted position of the diffuse maxima. Therefore, a renewed but detailed three-dimensional investigation seemed necessary using harder x rays to reduce the surface sensitivity. (Thermal neutrons are not attractive because the coherent elastic scattering is low in comparison with incoherent scatter-

ing, and the absorption is high, too.)

There are several other attractive features for investigating the gold-silver system. First, gold and silver form a solid solution for all compositions at room temperature. A possible dependence of the effective pair potentials on the composition or the presence of many-body interactions can thus be studied in detail for the same crystal structure. Secondly, for such a phase diagram one can calculate coherent low-temperature phases. Up to now, no ordered phase has been found experimentally. There are, however, various *ab initio* calculations, starting from $L1_2$ and $L1_0$ low-temperature phases (beside $A1$). The critical temperatures obtained for the order-disorder transitions[8-10] can be compared with Monte Carlo simulations based on effective pair potentials obtained from diffuse scattering experiments with samples in thermodynamic equilibrium. Thirdly, the lattice parameters of gold and silver only differ by less than 0.2%. Thus, no large diffuse scattering is expected from static atomic displacements. In contrast to the short-range-order scattering, this contribution can only be treated approximately, the approximation being best fulfilled for small scattering vectors and small static displacements.

THEORY

The coherent diffuse scattering from a binary A-B single crystal is due to the local deviations from the mean lattice, i.e., either to atomic displacements (static or dynamic) or to different types of atoms occupying the lattice sites. Within the framework of the kinematic theory, this diffuse scattering is often analyzed by introducing a series expansion for the displacements[11,12] (a more general cumulant expansion[13,14] would require modifications). For a cubic crystal one obtains approximately

$$I_{\text{diff}}(\mathbf{h}) = N c_A c_B |f'_A - f'_B|^2 \left[I_{\text{SRO}}(\mathbf{h}) + \sum_i h_i [\eta Q_i^{AA}(\mathbf{h}) + \xi Q_i^{BB}(\mathbf{h})] \right] + \sum_k I_k^{\text{TDS}}(\mathbf{h})$$

$$+ \text{higher-order static displacement terms} , \tag{1}$$

where h_i are the components of the scattering vector $\mathbf{h}$ in reciprocal-lattice units (r.l.u.) ($|\mathbf{h}|=2a\sin\theta/\lambda$, $\theta=$ half the scattering angle, $a=$ mean lattice parameter, $\lambda=$ wavelength of the incident radiation). Furthermore, $Nc_Ac_B|f_A'-f_B'|^2$ is called one Laue unit for the alloy with N atoms in the beam, while c_ν is the concentration and f_ν the atomic scattering factor of component $\nu(A,B)$. The prime with f_ν marks the inclusion of the thermal and (in principle) the static Debye-Waller factor. Ratios of the atomic scattering factors are given by η and ξ (see, e.g., Ref. 15), with

$$\eta=\mathrm{Re}[f_A'/(f_A'-f_B')] \ , \quad \xi=\mathrm{Re}[f_B'/(f_A'-f_B')] \ . \tag{2}$$

The short-range-order series $I_{\mathrm{SRO}}(\mathbf{h})$ is given by

$$I_{\mathrm{SRO}}(\mathbf{h})=\sum_l\sum_m\sum_n \alpha_{lmn}\cos(\pi h_1 l)\cos(\pi h_2 m)\cos(\pi h_3 n) \ , \tag{3}$$

where l,m,n are integers defining the interatomic vectors in units of half the translation vectors of the cubic unit cell. α_{lmn} are the Warren-Cowley short-range-order parameters

$$a_{lmn}=1-P_{lmn}^{AB}/c_B \ , \tag{4}$$

where P_{lmn}^{AB} is the probability of finding a B atom at site lmn if an A atom is at site 000.

The linear atomic displacement series in Eq. (1) are defined in a similar way, e.g.,

$$Q_1^{AA}(\mathbf{h})=-2\pi\sum_l\sum_m\sum_n(c_A/c_B+\alpha_{lmn})\langle(\Delta_1)_{lmn}^{AA}\rangle$$

$$\times\sin(\pi h_1 l)\cos(\pi h_2 m)$$

$$\times\cos(\pi h_3 n) \ . \tag{5}$$

$\langle(\Delta_i)_{lmn}^{AA}\rangle$ are the relative average static displacements in the i direction between two A atoms separated by an interatomic vector with components l,m,n. The Fourier series that are quadratic in the static displacements are usually considered for the higher-order static displacement terms;[16] these series will not be discussed in this paper. Finally, I_k^{TDS} is the thermal diffuse scattering of the kth order.

The Fourier series in Eq. (1) that explicitly refer to the atomic species can only be separated from one another if the scattering factor ratios vary in reciprocal space, as in the case of x-ray scattering. This analysis is called the Georgopoulos-Cohen method.[12] If there is no such variation of the scattering factor ratios (which holds for nuclear scattering with neutrons) the analysis of the diffuse scattering is based on the method due to Borie and Sparks.[11] In this case, the relative static displacements appear as combinations, e.g., only a first-order displacement coefficient γ_i^{lmn}

$$\gamma_i^{lmn}=-2\pi[\eta(c_A/c_B+\alpha_{lmn})\langle(\Delta_i)_{lmn}^{AA}\rangle$$

$$-\xi(c_B/c_A+\alpha_{lmn})\langle(\Delta_i)_{lmn}^{BB}\rangle] \tag{6}$$

is accessible. The number of Fourier series is thus reduced from 25 to 10. Both methods of evaluation were used in this paper.

If one expands the internal energy of a binary alloy in terms of correlation functions up to pair correlations, the expression reflecting the order of the alloy is

$$U=Nc_Ac_B\sum_l\sum_m\sum_n V_{lmn}\alpha_{lmn} \tag{7}$$

with $V_{lmn}=\frac{1}{2}(V_{lmn}^{AA}+V_{lmn}^{BB})-V_{lmn}^{AB}$. V_{lmn} are the effective pair potentials. Equation (7) is valid for a canonical ensemble; for a grandcanonical ensemble the change in concentration still has to be considered.

The effective pair potentials can be obtained from the atomic arrangement in various ways. In the following, two methods are employed. In the high-temperature approximation of Clapp and Moss,[17] the Fourier transformation of the pair potentials, $\widetilde{V}(\mathbf{h})$, is directly related to $I_{\mathrm{SRO}}(\mathbf{h})$ via

$$I_{\mathrm{SRO}}(\mathbf{h})=C/[1+2c_Ac_B\widetilde{V}(\mathbf{h})/(k_BT)] \ . \tag{8}$$

The normalization constant C is determined by $\Omega^{-1}\int I_{\mathrm{SRO}}(\mathbf{h})d\mathbf{h}=1$ with the integration over the unit cell Ω in reciprocal space as to satisfy $\alpha_{000}=1$.

Another method, the inverse Monte Carlo method introduced by Gerold and Kern,[18] is not limited to temperatures T sufficiently above the ordering temperature. This method is based on the property of the thermodynamic equilibrium that any observable will fluctuate statistically around its equilibrium value. Considering a large number of fluctuations, a nonlinear system of equations can be set up for the pair potentials. Whereas the inverse Monte Carlo method starts from a given atomic configuration, the Monte Carlo method[19] requires—within the present model of an Ising type of Hamiltonian—the knowledge of the effective pair potentials.

EXPERIMENTS

Au-Ag single crystals of three different compositions (nominally 1:3, 1:1, 3:1 for [Au]:[Ag]) were grown in graphite crucibles by the Bridgman technique; the starting alloys had been prepared from 99.99 materials (supplier: Métaux Précieux SA Metalor, Neuenburg, CH). Slices 10 or 12 mm in diameter and about 3 mm in thickness were cut by spark erosion. The concentration of the samples was determined from adjacent slices by the above-mentioned supplier. Possible concentration gradients of the samples along the crystal axes were, at most, 0.06 at. % Ag, that is just within the error bars of the analysis. The slices were homogenized for 2 d, heat treated for 7 d, and water quenched; the relevant data of the three alloys are summarized in Table I.

The temperatures T_h for homogenization were about 100 K below the solidus curve of the Au-Ag system. The aging temperatures T_a were chosen to ensure relaxation times for short-range ordering within 0.5–1.5 h.[20,21] Thus, it was possible to investigate a state of thermodynamic equilibrium after quenching.

To obtain a flat surface for the x-ray measurements, the slices were first mechanically polished (final polish with a diamond spray of 1 μm). The remaining damaged

TABLE I. Ag concentration c_{Ag}, temperature for homogenization, T_h, and for aging, T_a.

c_{Ag} (at. %)	T_h (K)	T_a (K)
24.99(5)	1223	488
47.74(3)	1203	502
74.65(4)	1173	513

surface layers were removed by electropolishing to restore a single-crystalline surface of minimal roughness.

The x-ray measurements were performed with Mo $K\alpha$ radiation (wavelength $\lambda = 0.071\,069$ nm) on a four-circle diffractometer using a symmetrical reflection geometry for the sample and a high-purity Ge detector. A sealed Mo tube operated at 44 mA and 50 kV was used; for further details of the experimental arrangement, see Ref. 15. The samples were mounted inside an evacuated Be hemisphere (50 mm in diameter) in order to remove air scattering in the immediate sample environment.

The diffuse scattering data were taken at room temperature at ~ 9500 positions under monitor control. Typically, 4500–12 000 counts were registered per position. A spacing of 0.1 r.l.u. was chosen, with scattering vectors ranging from 2.2 to 8.1 r.l.u. Symmetry-equivalent positions were selected, appropriate to a Georgopoulos-Cohen analysis.

The data were corrected for background and surface roughness; the latter correction was obtained from the decreasing intensity of the Au $L\alpha,\beta,\gamma$ fluorescence lines with smaller scattering angles 2θ. The data were converted to absolute units by comparing them with the scattering from polystyrene and pressed powders of Al and Ni, respectively.[16] The various calibrations agreed within $\pm 3\%$. The thermal diffuse scattering was calculated up to third order from nearest-neighbor force constants. These were determined from the elastic constants c_{ij} that were obtained from ultrasonic measurements using the pulse-echo-overlap method and cylindrical samples with a [110] axis. The data, together with B of the Debye-Waller factor $\exp[-2B(\sin\theta/\lambda)^2]$ determined according to Quimby and Sutton,[22] are summarized in Table II. Finally, the atomic scattering factors were taken from Doyle and Turner,[23] the corrections for anomalous scattering from Sasaki,[24] and the data for Compton scattering from Cromer and Mann.[25]

RESULTS

The short-range-order intensity was obtained by the separation methods of Georgopoulos and Cohen and of

TABLE II. Ag concentration c_{Ag}, elastic constants c_{ij} and B of the Debye-Waller factor.

c_{Ag} (at. %)	c_{11} (10^2 GPa)	c_{12} (10^2 GPa)	c_{44} (10^2 GPa)	B (10^{-2} nm^2)
24.9(4)	1.769(7)	1.428(9)	0.474(1)	0.697
47.8(3)	1.607(6)	1.258(7)	0.495(2)	0.609
78.1(1)	1.394(6)	1.061(6)	0.489(2)	0.631

Borie and Sparks. Strictly speaking, the requirement of the Borie-Sparks method, i.e., constant form factor ratios, is not fulfilled within the range of scattering vectors; e.g., for the linear displacement scattering these ratios vary up to about 35%. This is not a serious drawback if the displacement scattering is sufficiently weak. Furthermore, in the Borie-Sparks method, the number of Fourier series is reduced by a factor of 2.5. This should be advantageous in determining short-range-order scattering if the modulation in reciprocal space is sufficiently weak. As shown in the following, this situation is given in the Au-Ag system.

To stabilize the solution vector (the values of the various Fourier series for a set of symmetry-equivalent points) with both methods, the ridge regression technique[26] was applied in the separation procedure. The weighting of the norm of the solution vector with respect to the quality of the fit (R value) was set to 1 for the samples Au–25.0 at. % Ag and Au–47.7 at. % Ag and to 2 for Au–74.7 at. % Ag (see Ref. 27 for the criteria used).

The separated short-range-order intensities for the three alloys are shown in Fig. 1 within the $(h_1 h_2 0)$ plane. The hatched areas mark the regions around the Bragg reflections that were not considered in the evaluation because of the distinctly increased thermal diffuse scattering and the tails of the Bragg reflections. If one compares the results for both separation methods, three features are striking. First, a similar pattern of contour lines is seen, the one for the Georgopoulos-Cohen method looking more erratic. These larger variations might stem from the larger number of Fourier series. Secondly, whereas the intensities for the Ag-rich sample were not smoothed prior to plotting (over the nearest-neighbor intensities), this had to be done for the Au-rich sample. This might reflect problems related to the low penetration depth of x rays (2.3 μm for Au and 18.5 μm for Ag with Mo $K\alpha$ radiation). Thirdly, the maxima of the short-range-order intensity are always observed at 100-type positions. These are the positions of the superstructure reflections for the $L1_2$ and $L1_0$ structures (the latter without preferred alignment). The intensities are low, at most about 2 Laue units. This small modulation of the monotonic Laue scattering shows that only a low degree of short-range order is present.

To determine the Warren-Cowley short-range-order parameters, the 13 positions (out of the 146 distinguishable ones within the minimum separation volume), excluded because of their proximity to the Bragg reflections, were filled up with smoothly extrapolated intensities. These intensities were chosen constant, either 0.5 or 0.6 Laue units, depending on the alloy and the separation method used. The short-range-order parameters α_{lmn} were determined by a least-squares-fitting procedure. The appropriate number of Fourier coefficients was obtained by systematically increasing it until the following criteria were fulfilled: (1) the difference of the intensity recalculated from these coefficients and the separated short-range-order intensity no longer decreased decisively, and (2) not too many parameters were allowed to have values smaller than the standard deviations σ based solely on the statistical error of the measured inten-
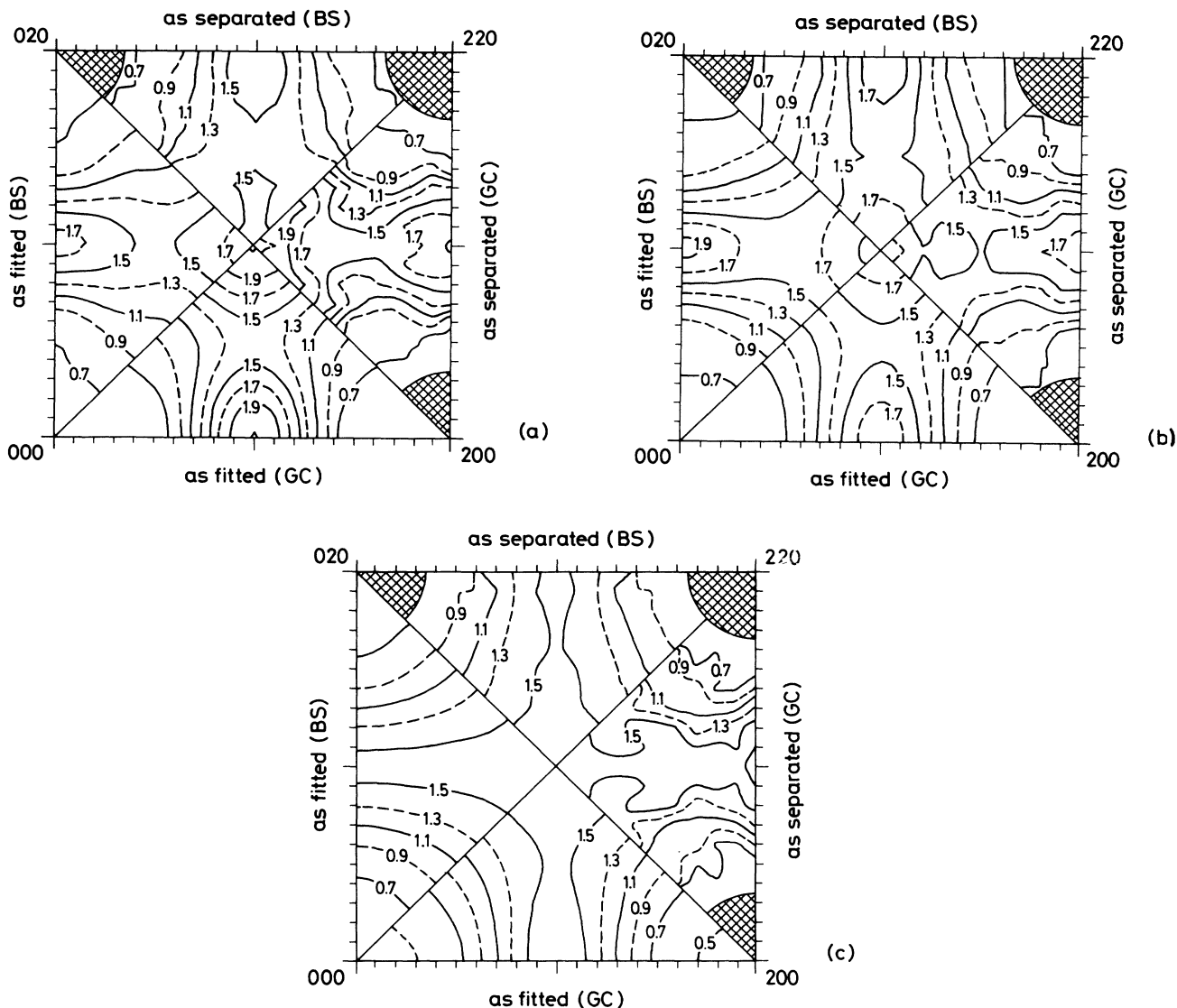
FIG. 1. Short-range-order intensity $I_{SRO}(\mathbf{h})$ in Laue units (isointensity lines) for a $(h_1 h_2 0)$ plane as separated and recalculated using the α_{lmn} values of Table III for (a) Au–25.0 at. % Ag, (b) Au–47.7 at. % Ag, (c) Au–74.7 at. % Ag.

sities.[27] The data are summarized in Table III. Also given are the extreme values these parameters may take for an ordered $L1_2$ or $L1_0$ superstructure, but with the present nonstoichiometric composition. It is seen that both evaluation techniques give similar results. The lower number of α_{lmn} determined with the Georgopoulos-Cohen method and their larger errors can be traced back to the larger number of Fourier series with that method. This is also seen in the R values of the fit defined by

$$ R = \sum_i |I_{SRO,i}^{sep} - I_{SRO,i}^{rec}| \Big/ \sum_i |I_{SRO,i}^{sep}| \, , $$

where the summation is over all positions within the minimum separation volume of the short-range-order intensity.

Theoretically, α_{lmn} is exactly 1 because there is either an A or a B atom at one site. Thus, the experimentally

determined value of α_{000} is often taken as a criterion to judge the quality of a measurement and its evaluation (see, e.g., Ref. 27) although $\alpha_{000} = 1$ is not a sufficient condition. The present results for α_{000} are always close to its theoretical value of 1. Deviations from 1 exceeding the given statistical error can be fully explained by, e.g., a different weighting factor in the ridge regression method (using a value of 2 instead of 1 will decrease α_{000} by 0.2 for Au–25.0 at. % Ag). Another reason for $\alpha_{000} > 1$ might be that the term

$$ N c_A c_B [|f_A - f_B|^2 - |f_A' - f_B'|^2] $$

was not introduced on the right-hand side of Eq. (1); the underlying approximation with this modification is discussed in Ref. 28. In fact, if one includes this term, α_{000} typically decreases by 7σ (about 0.11). The other α_{lmn}, however, decisive for the further evaluation, typically

TABLE III. Warren-Cowley short-range-order parameters α_{lmn} for (top) Au-25.0 at. % Ag, (middle) Au-47.7 at. % Ag, (bottom) Au-74.7 at. % Ag and for $L1_2$ or $L1_0$ long-range-ordered crystals with the same concentration. (GC: Georgopoulos-Cohen analysis, BC: Borie-Sparks analysis).

Shell index lmn	GC	BS	$L1_2$
000	1.0822(340)	1.0904(69)	1.0000
110	−0.0809(77)	−0.0677(28)	−0.3331
200	0.0279(89)	0.0328(26)	0.9994
211	0.0003(43)	0.0054(14)	−0.3331
220	0.0378(56)	0.0101(17)	0.9994
310	−0.0109(43)	−0.0049(14)	−0.3331
222		0.0043(20)	0.9994
321		−0.0005(9)	−0.3331
400		0.0016(22)	0.9994
330		−0.0099(16)	−0.3331
R value	0.248	0.080	

Shell index lmn	BC	BS	$L1_0$
000	1.0425(198)	1.1904(45)	1.0000
110	−0.0829(56)	−0.0810(21)	−0.3044
200	0.0411(66)	0.0270(19)	0.9132
211	0.0052(26)	0.0091(12)	−0.3045
220	0.0173(37)	0.0142(11)	0.9139
310	−0.0051(31)	−0.0080(11)	−0.3046
222		0.0019(11)	0.9135
321		−0.0020(7)	−0.3043
400		−0.0043(14)	0.9124
330		−0.0010(10)	−0.3048
411		0.0014(6)	−0.3043
420		0.0031(6)	0.9133
233		−0.0024(7)	−0.3044
R value	0.153	0.049	

Shell index lmn	GC	BS	$L1_2$
000	1.0933(140)	1.1447(32)	1.0000
110	−0.0836(43)	−0.0720(18)	−0.3271
200	0.0220(37)	0.0161(15)	0.9817
211	0.0086(20)	0.0089(9)	−0.3273
220	0.0121(25)	0.0046(7)	0.9818
310	−0.0036(23)	−0.0045(6)	−0.3272
R value	0.100	0.048	

vary just within $\pm\sigma$.

A variation of the smooth extrapolation of the short-range-order intensity towards the direct beam by ±0.2 Laue units only varies α_{lmn} within about 2σ. The value of α_{110} is always negative indicating short-range order. As seen in Table III, individual values of α_{110} are only 20–27 % those for the fully ordered alloy, indicating a low degree of short-range order. Comparing the sign sequence of the α_{lmn} with those of the $L1_2$ or $L1_0$ superstructure, the signs always differ first for α_{211}. A comparable tendency towards a positive or only slightly negative value of α_{211} was also observed with other short-

range-ordered alloys where the $L1_2$ superstructure is stable for the long-range-ordered state, e.g., Ni–10 at. % Al (Ref. 15) or Ni–23.5 at. % Fe (Ref. 29). This may be related to a larger fraction of elements of an antiphase boundary as discussed below.

To visualize the short-range order in real space, crystals were modeled on the computer, imposing the same concentrations and the same short-range-order parameters (within the uncertainties given in Table III). For comparison, crystals with a statistically uncorrelated arrangement were also created. Figure 2 shows (001) planes of Au–25.0 at. % Ag for both types of modeled crystals consisting of $32\times32\times32$ unit cells. The differences are subtle because the degree of short-range order is low. One can recognize that for the short-range-ordered crystal, Ag-Ag nearest neighbors are avoided and that there are localized features of the $L1_2$ superstructure. There are no signs of larger ordered particles within a disordered matrix, an arrangement that would be characteristic for the model of disperse order. This is not unexpected if one considers the limited number of relevant α_{lmn} and their low magnitude.

Modeled crystals were furthermore systematically searched for the 144 distinguishable arrangements within the first neighboring shell (Clapp configurations[30]). If
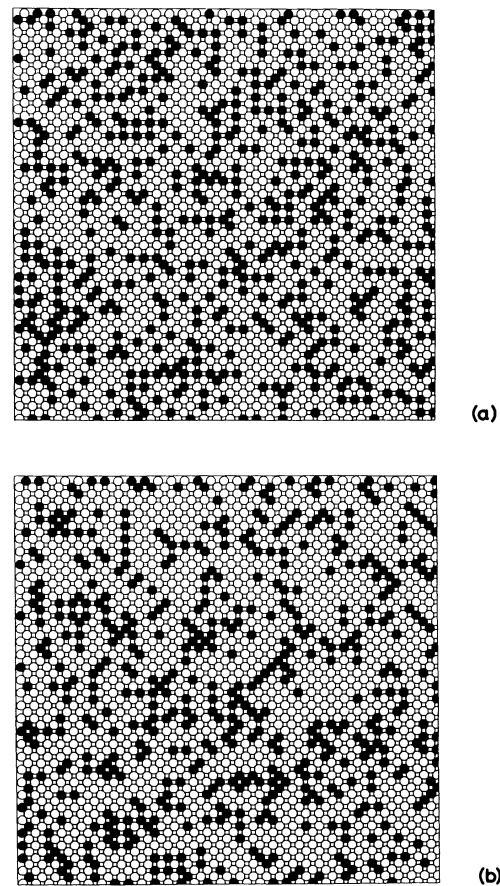

(a)

(b)

FIG. 2. (001) plane of Au–25.0 at. % Ag for (a) a modeled short-range-ordered sample and (b) a sample with a random distribution of Au ($\bigcirc$) and Ag ($\bullet$) atoms.

TABLE IV. Abundance (in %) for the Clapp configurations $C16$ and $C17$ (equal-type atoms in Au–47.7 at. % Ag and minority around majority atoms otherwise) for the short-range-ordered (SRO) alloy and for a random arrangement.

Configuration	Au–25.0 at. % Ag		Au–47.7 at. % Ag		Au–74.7 at. % Ag	
	Random	SRO	Random	SRO	Random	SRO
$C16$	0.1	0.5	0.1	0.6	0.1	0.4
$C17$	0.1	0.7	0.1	0.4	0.2	0.8

one considers the $L1_2$ or $L1_0$ features, one has to look for minority around majority atoms in the $L1_2$ and for minority around minority atoms (majority around majority atoms) in the $L1_0$ superstructure, especially in the $C16$ configuration (four nearest neighbors in a $\{100\}$ plane). For antiphase boundaries the crystals must be checked for the $C17$ configuration (involving two nearest neighbors each on two different sublattices). The abundance analysis just for these two configurations is shown in Table IV. Though these configurations are rare, both are distinctly larger for the short-range-ordered crystals. An increase of $C17$ is consistent with a positive value of α_{211}.

Beside the short-range-order intensity, the diffuse scattering due to the size effect was further analyzed. From the $Q_i^{\gamma\nu}$ and the $\eta Q_i^{AA}+\xi Q_i^{BB}$ terms, the Fourier coefficients of the first three shells were determined by a least-squares-fitting procedure. As an example the data of Au–47.7 at. % Ag are shown in Table V. Several features also seen with the two other alloys should be noted. First, the individual static atomic displacements between atoms of the same type, $(\Delta_i)_{lmn}^{\gamma\nu}$, are always negative. Approximating η and ξ by -0.97 and -1.97, respectively (their average values for the given range of scattering vectors), it is seen that $(\Delta_i)_{lmn}^{BB}/(\Delta_i)_{lmn}^{AA}\approx\eta/\xi$ for the leading coefficients. This results in a large compensation in γ_i^{lmn} as determined from Eq. (6). Thus, it is suspected that the ridge regression technique partly fails for the extraction of individual static atomic displacements. (No such distinct compensation was observed in systems with a larger change in lattice parameter with concentration, like Ni–10 at. % Al.[15]) Secondly, the values for γ_i^{lmn} calculated from the Georgopoulos-Cohen analysis are similar to the directly fitted γ_i^{lmn} of the Borie-Sparks analysis. This indicates that the intensity due to the static atomic displacements was properly considered when separating the short-range-order intensity. Owing to the large statistical error of the former ones,

however, their signs can be different, even for the largest γ_i^{lmn}. Finally, in comparison with the scattering due to short-range order, scattering due to the size effect varies typically within about ±0.3 Laue units near average scattering vectors of 4–6 r.l.u.

EFFECTIVE PAIR POTENTIALS

From the short-range-order intensity the effective pair potentials were determined by the approximation-free inverse Monte Carlo method as well as by the high-temperature approximation of Clapp and Moss. For the inverse Monte Carlo method, crystals of $16\times16\times16$ unit cells were modeled with the short-range-order parameters of Table III. About 70 000–110 000 virtual exchanges were considered and the change in pairs of minority around minority atoms registered for the various shells. The number of admitted effective pair potentials was systematically increased. By a subsequent Monte Carlo simulation the short-range-order intensity was recalculated and compared with the separated one. The result of such a recalculation is shown in Fig. 3 for Au–47.7 at. % Ag. It is found that the R value of the fitted and recalculated α_{lmn} (defined as described for I_{SRO}, see above) is within 1–2 %, and that the individual α_{lmn} values typically agree within about twice the standard deviation σ. This recalculation was based on the first three pair potentials. About three to four pair potentials turned out to be sufficient for the fitting. Because the effective pair potentials in a given shell are strongly affected by the short-range-order parameters of the same shell and because more distant shells are more strongly affected by the statistical fluctuations of the short-range-order intensity especially in the case of the Georgopoulos-Cohen analysis, it was decided to consider just three values of V_{lmn}. It should be noted that adding V_{220} will not decisively modify the V_{lmn} values of the first three shells; it will, however, be much more crucial when critical tem-

TABLE V. Static atomic displacements $\langle(\Delta_1)_{lmn}^{\gamma\nu}\rangle$ and the effective Fourier coefficients of the Georgopoulos-Cohen, γ_1^{lmn} (GC), and of the Borie-Sparks analysis, γ_1^{lmn} (BS), for Au–47.7 at. % Ag.

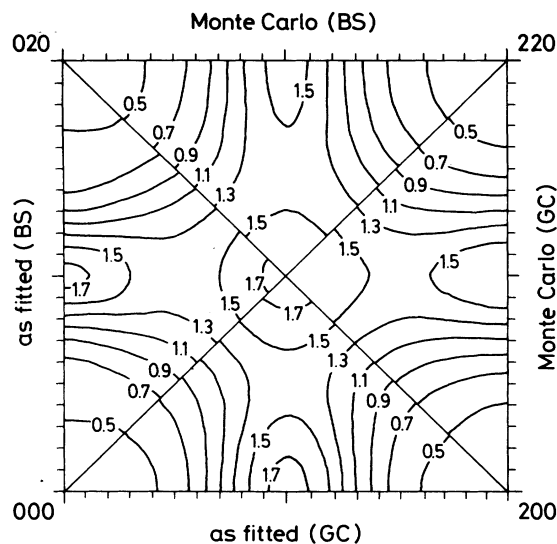| Shell index lmn	$\langle(\Delta_1)_{lmn}^{AgAg}\rangle$	$\langle(\Delta_1)_{lmn}^{AuAu}\rangle$	γ_1^{lmn} (GC)	γ_1^{lmn} (BS)
110	$-0.0100(10)$	$-0.0037(4)$	$-0.0043(71)$	$0.0046(6)$
200	$-0.0102(23)$	$-0.0036(9)$	$-0.0087(184)$	$-0.0027(19)$
211	$-0.0045(8)$	$-0.0013(4)$	$-0.0075(74)$	$-0.0010(6)$
121	$-0.0015(6)$	$-0.0003(3)$	$-0.0043(53)$	$-0.0009(4)$

FIG. 3. Short-range-order intensity $I_{SRO}(\mathbf{h})$ in Laue units for Au-47.7 at. % Ag recalculated from the α_{lmn} values of Table III (but $\alpha_{000}=1.0$) (as-fitted) and by a Monte Carlo simulation using the effective pair potentials of Table VI.

peratures for an order-disorder transition are determined. The effective pair potentials are summarized in Table VI. It is seen that there is a dominant V_{110} of 10–16 meV. The other ones are much lower. If one compares the V_{lmn} values obtained from the two different separation techniques (GC, BS in Table VI), an uncertainty of ± 2 meV is deduced. This error is similar to the one found with Ni-20 at. % Cr.[31] The error due to the differences in the various modeled crystals has much less influence: the uncertainties given in brackets are the standard deviations from five modeled crystals.

Effective pair potentials were also determined by the Clapp-Moss method. Starting from the α_{lmn} of Table III

in the determination of I_{SRO} they were then obtained by a Fourier transformation of $\tilde{V}(\mathbf{h})$. These effective pair potentials are only slightly smaller (by ~ 0.5 meV) than the ones found with the inverse Monte Carlo technique. Here, the constant in Eq. (8) was set to 1 as in Krivoglaz's derivation.[32] If one uses the normalization integral for C, all V_{lmn} are multiplied by ~ 0.89. This worsens the agreement with the result of the inverse Monte Carlo method. A similar dependence on C was found for short-range-ordered Ni-20 at. % Cr.[31] The use of the high-temperature approximation is justified in the present case, as the criterion $V_{110}/(k_B T) \ll 1$ is fulfilled [$V_{110}/(k_B T)$ ranges from 0.2 to 0.3, see Table VI].

Based on these sets of effective pair potentials, possible low-temperature phases were compared for their energy U [Eq. (7)]. The structures considered were $L 1_2$, DO_{22}, and DO_{23} for a concentration of 25 at. % and $L 1_0$ and "$1\frac{1}{2}0$" (see Ref. 33) for 50 at. %. These structures were chosen because their superreflections are in a region of low $\tilde{V}(\mathbf{h})$. The result for the ground states (lowest U) are given in Table VI. The $L 1_2$ and $L 1_0$ structures are dominantly found to represent these ground states. In the single case where a different result is obtained, the differences in U are within 0.1 meV for the various structures, in contrast to the distinctly larger differences observed otherwise. It is not surprising that the ground states are difficult to identify: if there is just one dominant pair potential, the ground state is nearly degenerate.

Monte Carlo simulations were used to determine the critical temperatures for the order-disorder transitions in the case of exact stoichiometry. The simulations were done for a canonical ensemble using a crystal of $16 \times 16 \times 16$ unit cells and periodic boundaries. The order parameter was determined starting at each temperature with a fully ordered alloy ($L 1_2$ or $L 1_0$). The critical temperatures—defined as those temperatures where long-range order has disappeared—are summarized in

TABLE VI. Effective pair potentials V_{lmn} (in meV) as determined by an inverse Monte Carlo method with the short-range-order parameters α_{lmn} from (top) Table III (GC: Georgopoulos-Cohen analysis, BS: Borie-Sparks analysis), (bottom) from Norman and Warren (Ref. 34) and Ziesemer (Ref. 35).

Shell index lmn	Au-25.0 at. % Ag		Au-47.7 at. % Ag		Au-74.7 at. % Ag	
	GC	BS	GC	BS	GC	BS
110	15.6(2)	10.4(1)	10.7(1)	10.4(1)	16.1(2)	12.2(2)
200	2.3(2)	$-1.0(1)$	$-0.1(1)$	0.7(1)	2.2(2)	1.0(1)
211	2.0(1)	0.2(1)	0.7(1)	0.4(1)	1.0(1)	0.2(1)
Ground	$L 1_2$	$L 1_2$	$L 1_2$	$L 1_2$	$L 1_2$	DO_{22}
states	$L 1_0$	$L 1_0$	$L 1_0$	$L 1_0$	$L 1_0$	$1\frac{1}{2}0$

Shell index lmn	Au-50 at. % Ag	Au-75 at. % Ag	Au-49.9 at. % Ag
	Norman and Warren		Ziesemer
110	11.4(1)	8.0(1)	12.5(1)
200	1.8(1)	$-0.1(1)$	$-1.9(7)$
211			$-0.4(3)$
Ground	DO_{22}	$L 1_2$	$L 1_2$
states	$1\frac{1}{2}0$	$L 1_0$	$L 1_0$

TABLE VII. Critical temperatures (in K) for the $L1_2$ and $L1_0$ order-disorder transitions based on the effective pair potentials of Table VI. The results of *ab initio* calculations are given in the last two lines.

	Au–25 at.% Ag	Au–50 at.% Ag	Au–75 at.% Ag
Table VI (BS)	155(5)	115(5)	115(5)
Table VI(GC)	210(5)	165(5)	165(5)
Norman *et al.*[34]			90(5)
Ziesemer[35]		168(21)	
Wei *et al.*[9]	200	240	120
Mohri *et al.*[10]	183	177	152

Table VII. The error bars refer to the step size used in raising the temperature. It is found that the critical temperatures are between 100 and 200 K. Systematically, these temperatures are somewhat lower for simulations based on the data from the Borie-Sparks analysis. The similarity of the critical temperatures for both alloys with the $L1_2$ superstructure directly indicates that many-body interactions are small.

DISCUSSION OF FORMER INVESTIGATIONS

Two previous investigations of diffuse x-ray scattering of Au-Ag single crystals are known.[34,35] In both cases the scattering in the $(h_1 h_2 0)$ plane of reciprocal space was measured, and no detailed three-dimensional measurements were reported.

As early as 1951, Norman and Warren[34] investigated Au–50 at.% Ag and Au–75 at.% Ag. The samples finally aged at 573 K for 4 weeks, most probably represented states of thermodynamic equilibrium [the relaxation time for short-range order is 17(9) s]. The effective pair potential V_{110} estimated from similar investigations in the Cu-Au system (where the approximation of Cowley[36] was used) was 7.7 meV, and a critical temperature of 160 K was deduced for the Au–75 at.% Ag sample (assuming the $L1_2$ structure). The present inverse Monte Carlo simulations based on α_{lmn} of Ref. 34 closely confirm the value of V_{110} (Table VI), but they indicate an overestimate of the critical temperature (Table VII). With the present low degree of short-range order, the agreement in V_{lmn} is not unexpected because, in the Cowley approximation, fluctuations in the distribution of atoms are ignored for the configurational entropy. The same overestimate in the critical temperature is obtained within the Bragg-Williams model.[37] In this model, the configuration energy has to include all relevant V_{lmn} values. In contrast to the Cowley model, the Bragg-Williams model starts directly from the sublattices of the long-range-ordered alloy, also neglecting any fluctuation on the various sublattices. In a more compact form than given by Cowley,[36] the following variation of the long-range-order parameter S with temperature is obtained

$$\ln \left[\frac{(1/3+S^2)(3+S^2)}{(1-S^2)} \right] = -\frac{2S^2}{k_B T} \tilde{V}(100) \ ,$$

from which the critical temperature is determined numerically. This result was also obtained by Khatchatu-

ryan[38] with the method of static concentration waves.

The second investigation is due to Ziesemer[35] and Ziesemer and Schüle.[7] The data considered to be the best[7] were obtained from Au–49.9 at.% Ag aged at 473, 523, and 573 K between 10 d and 1 h and then quenched [the relaxation times for short-range ordering vary from 10(5) h to 17(9) s]. Thus, states of thermodynamic equilibrium were once again investigated. For the sample aged at 573 K, effective pair potentials of $V_{110}=11.3$ meV and $V_{200}=-0.8$ meV were obtained[35] within the approximation of Cowley.[36] This time, again, the values for the effective pair potentials are close to the present results obtained by the inverse Monte Carlo method (Table VI, the error in this case is the standard deviation from averaging the potentials obtained for each aging temperature). The critical temperature estimated to 290 K in Ref. 35 is again too high in comparison with the present Monte Carlo simulations. Because of this high value, a higher short-range-order intensity was expected at a lower temperature [samples were also irradiated at 328 K, i.e., at a temperature within stage III (see Ref. 39), where vacancies are mobile within the one-interstitial model], but not observed experimentally. Thus, Ziesemer and Schüle concluded that the model of statistical short-range order is incorrect and that disperse order is present. Their interpretation was "that the particle size decreases while the degree of order within the particles increases with decreasing temperature." With the present critical temperature of 140(25) K (and also based on Monte Carlo simulations at 328 K), this discrepancy is distinctly reduced. There is thus no need to invoke the idea of disperse order.

Ab initio calculations of the phase diagram have also been reported.[9,10] Whereas the earliest attempts to determine theoretically the critical temperature for Au–50 at.% Ag ($L1_0$-ordered phase) obviously failed[8]—this calculation only considered a single s band neglecting d bands—later calculations resulted in critical temperatures below room temperature. These calculations by Wei *et al.*[9] and by Mohri *et al.*[10] parametrized the internal energy by a Hamiltonian with only nearest-neighbor interactions but considering pair, triplet, and quadruplet interactions. For the configurational entropy, the tetrahedron approximation of the cluster variation method was taken. Critical temperatures were calculated for the $L1_2$- and $L1_0$-ordered phases; they are also given in Table VII. Both theoretical data sets—based on different procedures to calculate the internal energy—are

rather similar. They both show that the lowest transition temperature occurs for Au–75 at. % Ag. This is consistent with the present Monte Carlo simulations. The small differences in the critical temperatures for both $L1_2$ phases also show that many-body interactions are small.

Although in the present work detailed three-dimensional diffuse scattering data were taken using harder x-rays in contrast to previous investigations (with Cu $K\alpha$ radiation) and looking for the three stoichiometric compositions of interest, the data obtained for the effective pair potentials are not too different from the former results. They even agree concerning the critical temperatures, if the approximation-free inverse Monte Carlo method is used. It seems that, because of the small degree of short-range order, the precision in the determination of the effective pair potentials will not dis-

tinctly improve even if electron irradiation is used to establish larger modulations in the short-range-order scattering at a temperature where vacancies are mobile. From the present results it can be concluded that diffuse scattering provides no compelling reason to resort to the model of disperse order in Au-Ag.

[1]W. Schüle and G. Crestoni, Z. Metallkde. **66**, 728 (1975).

[2]M. D. Giardina, W. Schüle, W. Frank, and A. Seeger, Radiat. Eff. **12**, 277 (1972).

[3]K. Lücke and H. Haas, Scr. Metall. **7**, 781 (1973).

[4]J. M. Cowley, J. Appl. Phys. **21**, 24 (1950).

[5]H.-P. Aubauer, Acta Metall. **20**, 165 (1972).

[6]H. Thomas, Z. Phys. **129**, 219 (1951).

[7]K. Ziesemer and W. Schüle, Acta Metall. **33**, 587 (1985).

[8]R. C. Kittler and L. M. Falicov, Phys. Rev. B **19**, 527 (1979).

[9]S.-H. Wei, A. A. Mbaye, L. G. Ferreira, and A. Zunger, Phys. Rev. B **36**, 4163 (1987).

[10]T. Mohri, K. Terakura, S. Takizawa, and J. M. Sanchez, Acta Metall. Mater. **39**, 493 (1991).

[11]B. Borie and C. J. Sparks, Acta Crystallogr. A **27**, 198 (1971).

[12]P. Georgopoulos and J. B. Cohen, J. Phys. (Paris) Colloq. **38**, C7-191, (1977).

[13]N. H. March, S. W. Wilkins, and J. E. Tibballs, Cryst. Lattice Defects **6**, 253 (1976).

[14]S. Dietrich and W. Fenzl, Phys. Rev. B **39**, 8873 (1989).

[15]F. Klaiber, B. Schönfeld, and G. Kostorz, Acta Crystallogr. A **43**, 525 (1987).

[16]L. H. Schwartz and J. B. Cohen, *Diffraction from Materials* (Springer, Berlin, 1987), pp. 402 and 542.

[17]P. C. Clapp and S. C. Moss, Phys. Rev. **142**, 418 (1966).

[18]V. Gerold and J. Kern, Acta Metall. **35**, 393 (1987).

[19]K. Binder, in *Monte Carlo Methods in Statistical Physics*, edited by K. Binder (Springer, Berlin, 1979), p. 1.

[20]S. Radelaar, Phys. Status Solidi **27**, K63 (1968).

[21]T. Doppler and W. Pfeiler (private communication).

[22]S. L. Quimby and P. M. Sutton, Phys. Rev. **91**, 1122 (1953).

[23]P. A. Doyle and P. S. Turner, Acta Crystallogr. A **24**, 390 (1968).

[24]S. Sasaki (unpublished).

[25]D. T. Cromer and J. B. Mann, J. Chem. Phys. **47**, 1892 (1967).

[26]C. L. Lawson and R. J. Hanson, *Solving Least Squares Problems* (Prentice-Hall, New Jersey, 1974), p. 190.

[27]T. B. Wu, E. Matsubara, and J. B. Cohen, J. Appl. Cryst. **16**, 407 (1983).

[28]B. E. Warren, *X-Ray Diffraction* (Dover, New York, 1990), p. 237.

[29]S. Lefèbvre, F. Bley, M. Fayard, and M. Roth, Acta Metall. **29**, 749 (1981).

[30]P. C. Clapp, Phys. Rev. B **4**, 255 (1971).

[31]B. Schönfeld, L. Reinhard, G. Kostorz, and W. Bührer, Phys. Status Solidi B **148**, 457 (1988).

[32]M. A. Krivoglaz and A. A. Smirnov, *The Theory of Order-Disorder in Alloys* (MacDonald, London, 1964), p. 345.

[33]P. C. Clapp, and S. C. Moss, Phys. Rev. **171**, 754 (1968).

[34]N. Norman and B. E. Warren, J. Appl. Phys. **22**, 483 (1951).

[35]K. Ziesemer, Ph.D. thesis, Universität Frankfurt, 1976.

[36]J. M. Cowley, Phys. Rev. **77**, 669 (1950).

[37]W. L. Bragg and E. J. Williams, Proc. R. Soc. London, Ser. A **145**, 699 (1934).

[38]A. G. Khachaturyan, Prog. Mater. Sci. **22**, 1 (1978).

[39]B. Sprušil, H. Haas, and H. Wollenberger, Radiat. Eff. **5**, 273 (1970).